Journal of Power Sources 217 (2012) 373–380

Contents lists available at SciVerse ScienceDirect

Journal of Power Sources

journal homepage: www.elsevier.com/locate/jpowsour

# Alkali resistant and conductive guanidinium-based anion-exchange membranes for alkaline polymer electrolyte fuel cells

Xiaocheng Lin [a], Liang Wu [a], Yanbo Liu [a], Ai Lien Ong [b], Simon D. Poynton [b], John R. Varcoe [b], Tongwen Xu [a,*]

[a] CAS Key Laboratory of Soft Matter Chemistry, Laboratory of Functional Membranes, School of Chemistry and Materials Science, University of Science and Technology of China, Hefei, Anhui 230026, PR China
[b] Department of Chemistry, Faculty of Engineering and Physical Sciences, The University of Surrey, Guildford GU2 7XH, United Kingdom

## HIGHLIGHTS

- Alkaline anion exchange membranes (AAEMs) with guanidium groups were prepared.
- The ionic conductivity of AAEMs can attain as high as 71 mS $cm^{-1}$.
- The membranes are stable after immersion in 1 M KOH solution at 25 °C for 8 d.
- The membranes show promise for application in alkaline polymer electrolyte fuel cells.

## ARTICLE INFO

*Article history:*
Received 14 March 2012
Received in revised form
15 May 2012
Accepted 18 May 2012
Available online 12 June 2012

*Keywords:*
Anion-exchange membrane fuel cells
Guanidinium groups
Alkali stability
Ionic conductivity

## ABSTRACT

Novel alkaline anion-exchange membranes (AAEMs) containing pendant guanidinium groups are synthesized from poly(2, 6-dimethyl-1,4-phenylene oxide) (PPO) by benzyl bromination and subsequent reaction with 1,1,2,3,3-pentamethylguanidine (PMG). The performances of the resultant guanidinium-functionalized-PPO (GPPO) AAEMs are controlled by tailoring the amount of guanidinium groups in the membrane matrix. The AAEMs exhibit high ionic conductivities (up to 71 mS $cm^{-1}$ at room temperature); this stems from the high alkalinity (high $pK_a$) of guanidinium hydroxide, which leads to an augmentation of both the number of dissociated hydroxides and water molecules. Furthermore, the GPPO AAEMs exhibit excellent thermal and alkali stabilities due to the presence of the $\pi$ electron conjugated systems of the pendant guanidinium head-groups permitting the positive charge to be delocalized over one carbon and three nitrogen atoms. Specifically, the initial decomposition temperatures, from thermogravimmetric analyses of the GPPO AAEMs, are high at 270 °C, while the hydroxide conductivity of the AAEM with the most optimal properties remains stable in aqueous KOH (1 mol $dm^{-3}$) solution for 192 h at 25 °C. A $H_2/O_2$ fuel cell test at 50 °C with a GPPO AAEM yielded a beginning-of-life peak power density of 16 mW $cm^{-2}$.



## 1. Introduction

Polymer electrolyte membrane fuel cells are attracting increasing attention as a clean energy generation technology due to their high energy conversion efficiencies, low local pollution levels, low noise and low maintenance costs [1]. Recently, fuel cells containing anion-exchange polymer electrolyte (APEFCs) are gaining international recognition as they promise to overcome the disadvantages of Nafion-based proton exchange membrane fuel cells (PEMFCs) such as low CO tolerance, high electro kinetic over potentials, high fuel permeation and catalyst cost [2]. The existence of an alkaline environment in APEFCs presents several advantages compared with PEMFCs: Enhanced cell efficiency, expanded range of the viable cathode catalysts and fuels, depressed fuel crossover and more facile fuel oxidation [1,3–7]. These advantages increase the probability of reducing the costs of APEFCs compared to the better known PEMFCs.

Over the last 10 years, alkaline anion-exchange membranes (AAEMs), the core component of APEFCs, have been extensively studied and considerable advances have been made [1,8]. Among the variety of methods used for AAEM synthesis, an important and common method is to modify an existing base polymer, such as poly(phthalazinon ether sulfone ketone) (PPESK) [9], polysulfone

* Corresponding author. Tel.: +86 551 3601587; fax: +86 551 3601592.
*E-mail address:* twxu@ustc.edu.cn (T. Xu).

0378-7753/$ – see front matter © 2012 Elsevier B.V. All rights reserved.
http://dx.doi.org/10.1016/j.jpowsour.2012.05.062

(PS) [10] and poly(ether ketone) (PEK) [11]. Typically, the AAEMs are synthesized via chloromethylation of the pristine polymers and subsequent exposure to trimethylamine (TMA) to form the desired benzyltrimethyl-type quaternary ammonium (QA) head-groups [9–11]. However, there are three potential disadvantages with the use of AAEMs: (1) The commonly used chloromethyl methyl ether, used for the chloromethylation step, is a carcinogen and highly harmful to human health (its use has been restricted since 1970s) [12]; (2) The poor stability of the QA head-groups (the most commonly encountered) in alkaline environments is caused by the attack on the quaternary ammonium groups by the strongly nucleophilic $OH^-$ anions via direct nucleophilic displacements, Hofmann elimination reactions, and/or minor side-reactions involving ylide-intermediates [1,13–15]; (3) The lower ionic conductivities observed are due to the weak alkalinity of QA hydroxides (*cf.* the strong acidity of the perfluorosulfonic acid groups in PEMs) and resultant poor self-dissociation capability (*e.g.* trimethylamine has a $pK_a = 10.8$), as well as anion mobilities that are generally lower than the mobility of protons [16].

An obvious target to solve these problems is to develop AAEMs with superior alkali stabilities and ionic conductivities, whilst avoiding excessive swelling (when hydrated) and the use of chloromethyl methyl ethers. To achieve this aim, a series of AAEMs with pendant guanidinium groups were prepared, as recent reports suggest that this head-group exhibits appealing alkali stability and high anion (including hydroxide) conductivities (due to the high basicity and delocalized structure of the guanidinium functional groups) [17]. The AAEMs in the prior report were prepared using chloromethylation reactions followed by reaction with 1,1,2,3,3-pentamethylguanidine (PMG) [17]. It should be noted that PMG possesses a $pK_a = 13.8$ [16], which is much higher than that of trimethylamine; this suggests that guanidinium hydroxides will express enhanced $OH^-$ anion dissociation. This higher alkalinity promises an augmentation of both the number of dissociated hydroxides and their associated water molecules, thereby facilitating hydroxide ion conduction [17]. In addition, the guanidinium groups can take part in conjugation and are strong electron donors, both of which enhance their alkaline and thermal stabilities [17]. Therefore, the use of guanidinium head-groups addresses two major issues (alkaline stability and hydroxide conductivity). However, the problem regarding the use of chloromethyl methyl ether synthesis reagent remains to be resolved. Therefore, AEMs were prepared with pendant guanidinium groups attached to poly(2,6-dimethyl-1,4-phenylene oxide) (PPO), a system that, to the best of our knowledge, has not been studied to date. According to our extensive previous work, brominated PPO (BPPO) can be easily formed using simple bromination reaction and as such allows the avoidance of the use of chloromethyl methyl ethers [18]. Besides, PPO is thermally stable with a high glass transition temperature (273 °C) and so can be used in applications requiring relatively high temperatures [19]. Therefore, the target AAEMs are expected to present three benefits: (1) a lower toxicity fabrication process; (2) enhanced alkali stabilities compared to QA-type AAEMs; and (3) enhanced alkali anion conductivities.

The AAEMs in this study were prepared from PPO using a benzyl bromination reaction followed by reaction with PMG. This synthetic process will be investigated in detail and the reaction conditions targeted to produce AAEMs with optimal fuel cell relevant properties. The PPO-guanidinium AAEMs (designated GPPO) were characterized for ionic conductivity, alkali stability, ion exchange capacity (IEC), and water content ($W_R$) as well as being evaluated in a simple $H_2/O_2$ fuel cell (beginning-of-life test). To directly demonstrate the superiority of the GPPO AAEMs, they were compared with benchmark AAEMs containing quaternary trimethylammonium groups (designated QPPO) and with a similar IEC.

## 2. Methodology

### 2.1. Materials

Poly(2,6-dimethyl-1,4-phenylene oxide) (PPO) of intrinsic viscosity = 0.57 dl $g^{-1}$ in chloroform at 25 °C was kindly provided by Tianwei Membrane Company (Shandong, P.R. China). 1,1,3,3-tetramethylurea (TMU) was purchased from Aladdin Scientific Co. Ltd. (Shanghai, P.R. China). Toluene and acetonitrile solvents were dried by refluxing over $CaH_2$ (s) and distilled prior to use. All other reagents were of analytical grade and used as received.

### 2.2. Synthesis of 1,1,2,3,3-pentamethylguanidine (PMG)

The Vilsmeyer salt (*C*-chloro-*N*,*N*,*N*′*N*′-tetramethylformamidine) was prepared via the reaction of TMU with oxalyl chloride in toluene under a $N_2$ atmosphere: $^1H$ NMR ($CD_3Cl$) $\delta_H = 3.54$ (6H, s). Excess methylamine gas was then slowly bubbled through the solution of Vilsmeyer salt in dry acetonitrile at room temperature for 24 h [17]. After the solution was refluxed for 6 h, 4 equivalents of NaH were added with vigorous stirring. The solution, recovered after filtration, was then distilled under reduced pressure to yield PMG (53% yield).

### 2.3. Synthesis of benzyl brominated poly(2,6-dimethyl-1,4-phenylene oxide) (BPPO)

BPPO was prepared as previously reported [18]. In summary, PPO was dissolved in chlorobenzene to form an 8% m/v solution and bromination reaction was conducted by adding bromine dissolved in cholorobenzene (33% v/v) at 130 °C for 8 h. The BPPO was precipitated on addition of methanol, washed and dried at 80 °C for at least 20 h. The degree of bromination was controlled by the amount of bromine added and was measured using $^1H$ NMR. The degree of benzyl bromination of the polymers was denoted as *X* in the polymer designations BPPO-*X* (intermediate brominated polymers) and GPPO-*X* (the final AAEMs: see Table 1 for details).

### 2.4. Synthesis of the guanidinium AAEMs (GPPO)

GPPO was obtained by the reaction of BPPO-*X* with PMG in N-methyl-2-pyrrolidone (NMP) to yield the desired AAEMs. An exemplar synthesis is as follows: BPPO-0.42 (1.0 g, 2.7 mmol of $-CH_2Br$) was dissolved in 40 $cm^3$ NMP to form a 2.5% m/v solution. PMG (0.73 g, 5.4 mmol) was then added and the solution was stirred at room temperature for 24 h. The solution was concentrated by evaporation at 65 °C for 8 h to form an 8% m/v solution. The final solution was cast on Teflon plate for solvent volatilization to yield the GPPO-0.42 anion-exchange membrane in the $Br^-$ anion-form (typical thickness = 18 μm). The GPPO-0.42 membrane was treated alternately (2 times each) with aqueous HCl (1.0 mol $dm^{-3}$) solution and aqueous NaOH (2.0 mol $dm^{-3}$) solution, followed by thorough washing with (grade I) distilled

**Table 1**
Summary of the synthesis of the GPPO-*X* AAEMs.

| Sample | Molar ratio of $Br_2$ to benzyl (%) | Benzyl bromination degree (%) | Membrane denotation |
|---|---|---|---|
| #1 | 7.5 | 5 | GPPO-0.05 |
| #2 | 15 | 9 | GPPO-0.09 |
| #3 | 25 | 22 | GPPO-0.22 |
| #4 | 35 | 30 | GPPO-0.30 |
| #5 | 50 | 42 | GPPO-0.42 |
| #6 | 60 | 54 | GPPO-0.54 |

water. This yielded the GPPO-0.42 AAEM (in predominantly the hydroxide form). $^1$H NMR data indicated that the conversion rate of $-CH_2Br$ was nearly 100%.

### 2.5. Synthesis of the benchmark QA AAEM (QPPO)

The QPPO benchmark AAEM was prepared from BPPO-0.42 which was quaternized as follows: BPPO-0.42 was immersed in excess aqueous trimethylamine (TMA, 1 mol dm$^{-3}$) solution for 8 d at room temperature to ensure the full conversion of $-CH_2Br$ to QA groups. The resultant QPPO-0.42 anion-exchange membrane in the $Br^-$ form was then converted to the hydroxide form as described above.

### 2.6. Characterizations

#### 2.6.1. Spectroscopic characterization

$^1$H spectra were recorded on an AV III 400 NMR spectrometer ($^1$H resonance at 400 MHz, Bruker). Infrared spectra were recorded on a Vector 22 FT-IR spectrometer (Bruker).

#### 2.6.2. Thermogravimmetric analysis (TGA)

TGA thermograms were recorded on a Shimadzu TGA-50H analyzer under nitrogen flow and with a heating rate of 10 °C min$^{-1}$. This technique gives an indication of the short-term thermal properties and stabilities of the polymers.

#### 2.6.3. Tensile properties

The tensile properties were measured on an Instron universal tester (Model 1185) at 25 °C with dumbbell shaped specimens and a crosshead speed of 25 mm min$^{-1}$ (initial gauge length = 25 mm). The tensile strength (TS) and elongation at break ($E_b$) values were recorded.

#### 2.6.4. Determination of ion-exchange capacities (IECs)

The ion-exchange capacities were measured as in previous studies [18]. The AAEM sample was dried to a constant mass and then converted to the $Cl^-$ anion form by immersion in aqueous NaCl (1 mol dm$^{-3}$) solution. Thorough washing with distilled water was conducted to remove the excess NaCl. The sample was then immersed in aqueous $Na_2SO_4$ (0.5 mol dm$^{-3}$) solution for 2 d. The amount of $Cl^-$ anions released from the polymer sample was then determined by titration with aqueous $AgNO_3$ (0.1 mol dm$^{-3}$) solution using $K_2Cr_2O_7$ as an indicator. The IEC value was calculated as the amount $Cl^-$ (in mmol) per g of dry membrane (1:1 reaction ratio between the $Cl^-$ anions and $Ag^+$).

#### 2.6.5. Water uptake ($W_R$) and linear expansion ratio (LER)

Gravimmetric water uptake ($W_R$) was measured according to our previous work as an empirical measure of the hydrophilicity of the GPPO-*X* membranes [18]. The samples were dried in vacuum at 80 °C until a constant weight $m_{dry}$ was attained. The samples were then immersed in distilled water for 2 d, after which water was quickly removed from the surfaces of the samples and the mass of the samples were recorded ($m_{wet}$). The $W_R$ was calculated according to equation (1):

$$W_R = \frac{m_{wet} - m_{dry}}{m_{dry}} \times 100\% \quad (1)$$

The linear expansion ratio (LER) was used to characterize the swelling ratio of membranes, which was determined from the differences between wet and dry dimensions of a membrane sample (dry samples were originally *ca.* 4 cm in length ($L$) and 1 cm in width). The LER values were calculated according to equation (2) [20]:

$$LER = \frac{L_{wet} - L_{dry}}{L_{dry}} \times 100\% \quad (2)$$

#### 2.6.6. Determination of the ionic conductivities

The ionic conductivities of the GPPO-*X* AAEMs were measured using the commonly encountered four-point probe technique [21]. The Teflon measuring cell consisted of two stainless steel flat outer current-carrying electrodes (spacing = 2 cm) and two platinum wire inner potential-sensing electrodes (spacing = 1 cm). The AAEMs samples (1 cm × 4 cm) were fully hydrated and quickly mounted into the cell. The impedance was recorded using an Autolab® PGSTAT 302 (Eco Chemie, Netherlands) in galvanostatic mode (a.c. current amplitude = 0.1 mA, frequency range = 1 MHz to 50 Hz). Bode plots were used to determine the frequency region over which the magnitude of the impedance was constant; the ionic resistance was then obtained from the associated Nyquist plot. The ionic conductivities recorded are likely to be due to a mixture of alkaline anions ($OH^-$ and either $HCO_3^-$ or $CO_3^{2-}$) as the $OH^-$ forms of the GPPO-*X* membranes will have reacted with $CO_2$ in the air during cell mounting and impedance measurement.

The ionic conductivities ($\kappa$) were calculated according to equation (3):

$$\kappa = \frac{L}{RWd} \quad (3)$$

where $R$ is the membrane resistance (Ω), $L$ is the distance between potential-sensing electrodes (cm), and $W$ and $d$ are the width and thickness of the membrane (cm) respectively.

#### 2.6.7. Estimation of the alkali stabilities

The alkali stabilities of GPPO-*X* AAEMs were investigated as reported previously [17]. Specifically, the samples were treated with aqueous KOH (1 mol dm$^{-3}$) solution at room temperature for increasing lengths of time. After this high pH treatment regimen, the membranes were immersed in distilled water for 48 h to remove the residual (excess) KOH and the ionic conductivities were again measured.

#### 2.6.8. Performance of an alkaline membrane fuel cell

Fuel cell testing was conducted according to previous reports [22,23].

*2.6.8.1. Membrane electrode assembly.* Catalyst inks were prepared by first mixing the Pt catalyst (HISPEC 3000: 20 wt% Pt/Vulcan$_{XC\text{-}72R}$, Johnson Matthey Plc. UK) and poly(vinylbenzyl chloride) with ethyl acetate solvent. After the mixture was sonicated for at least 30 min in ultrasonic water-bath, the ink was carefully sprayed onto the microporous layer coating (20%mass PTFE binder, 1 mg$_{carbon}$ cm$^{-2}$) on one side of a wet-proofed carbon paper gas diffusion substrate (20%mass PTFE wet-proofing) until a Pt loading of 0.40 mg cm$^{-2}$ was achieved. A poly(vinylbenzyl chloride) loading of 15%mass, with respect to the mass of Pt/C catalyst powder, was used. The dried poly(vinylbenzyl chloride)-treated gas diffusion electrodes (identical anode and cathodes were used) were subsequently treated with undiluted *N*,*N*,*N*′,*N*′-tetramethyl-1,6-hexanediamine (99%, Sigma–Aldrich) overnight. This is Surrey's 1st generation ionomer concept (designated SION1) [24]. After washing with DI water, the electrodes were converted to $OH^-$ as for the GPPO-*X* membrane synthesis. GPPO-0.54 AAEM was then sandwiched between the two electrodes, with catalyst layer facing the AAEM, and the resultant MEA was assembled into the fuel cell fixture without hot-pressing.

*2.6.8.2. Fuel cell testing.* The performances of MEA (electrode geometric area of 5.3 $cm^2$) were measured in a Scribner 850e fuel cell test station (Scribner Associates Inc., USA) without back pressurization of the gas supplies. The test cell comprised a pair of graphite bipolar plates, machined with serpentine flow fields, two gold-coated current collector plates and two stainless steel end plates for holding the bipolar plates in place. Rod heaters were inserted into the end plates to control the cell temperature. The prepared MEAs were correspondingly sandwiched in between two gaskets (thickness = 0.15 mm) and sealed into the test cell at a constant torque of 5.5 N m, using retaining bolts and a torque driver. A Fuel Cell® software ver. 4 (Scribner Associates) was used to record the galvanostatic polarization curves of fuel cell. The input flow rates of anode $H_2$ (industrial grade, BOC) and cathode $O_2$ (industrial grade, BOC) were respectively controlled at 600 $cm^3$ $min^{-1}$. The humidification temperatures of anode and cathode were controlled at the cell temperature of 50 °C, achieving the calculated relative humidity (RH) = 100%. Prior to polarization curve measurement, the assembled cells were activated operation of the cell at open circuit voltage (OCV) for 1 h, followed by potentiostatic control at 0.1 V and then 0.5 V for 30 min each (or until a stable constant current was obtained).

## 3. Results and discussions

### 3.1. NMR

The synthesis of PMG, BPPO, and GPPO is presented in Scheme 1 and their chemical structures were confirmed by $^1H$ NMR measurements. The NMR spectrum ($CDCl_3$) of the TMU starting material for PMG synthesis (Fig. 1(a)) consists of one singlet at $\delta_H = 2.81$ whilst the spectrum of PMG (Fig. 1(b)) consists of three singlets at $\delta_H = 2.93$, 2.76, and 2.64 of relative intensity 1:2:2 [25].

As mentioned above, BPPO was prepared via the benzyl bromination of PPO and the molar ratio of bromine reacted, with respect to the PPO repeat unit, is the controlling factor for the degree of benzyl bromination. The molar ratio of $Br_2$ to the BPPO repeat unit was varied from 7.5% to 60% and the $^1H$ NMR spectra (Fig. 2) were recorded to measure the resultant degree of the benzyl bromination in each case. For the $^1H$ NMR spectrum of PPO (Fig. 2a), the signals with chemical shifts $\delta$ = 6.4–6.5 were assigned to aromatic hydrogens, while the signals at $\delta$ = 2.0–2.1 were assigned to the benzyl (-$CH_3$) hydrogens [18]. The spectrum for BPPO-0.54 (Fig. 2b) exhibited new signals at $\delta$ = 4.0–5.0, which were assigned to the hydrogens of benzyl bromide (–$CH_2Br$) [18]; these signals were used to calculate the *X* values of the BPPO-*X* (summarized in Table 1).

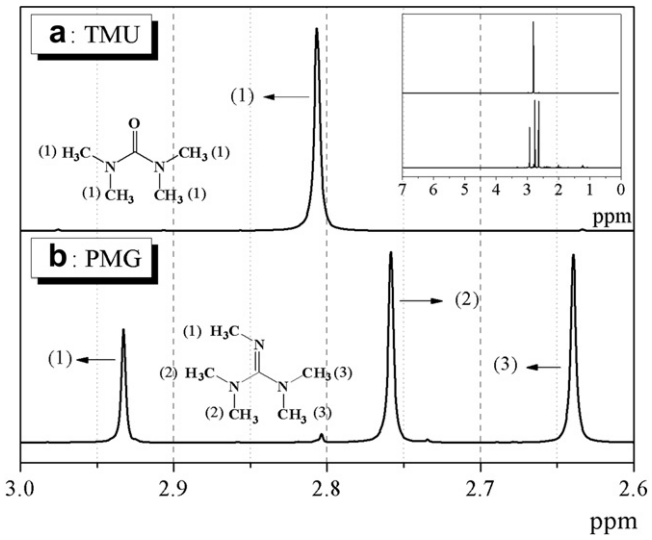


**Fig. 1.** The NMR spectra of (a) TMU, (b) PMG.

GPPO-*X* AAEMs were prepared via the reaction of the BPPO-*X* intermediate membranes with PMG. The molar ratio of PMG:–$CH_2Br$ groups of the BPPO was controlled at 2:1 to ensure that the benzyl bromide (–$CH_2Br$) was fully converted into the desired guanidinium functional groups. The $^1H$ spectrum (Fig. 2c) for GPPO-0.54 was used to measure the degree of the quaternization. Resonances due to guanidinium groups were detected as the new signals at $\delta$ = 2.6–3.3 [17]: The degree of conversion was close to 100%.

### 3.2. FT-IR

FT-IR was employed to study the functional chemistries of the various membranes and to confirm that the reactions that had taken place as expected (Fig. 3). Fig. 3a presents the spectrum of

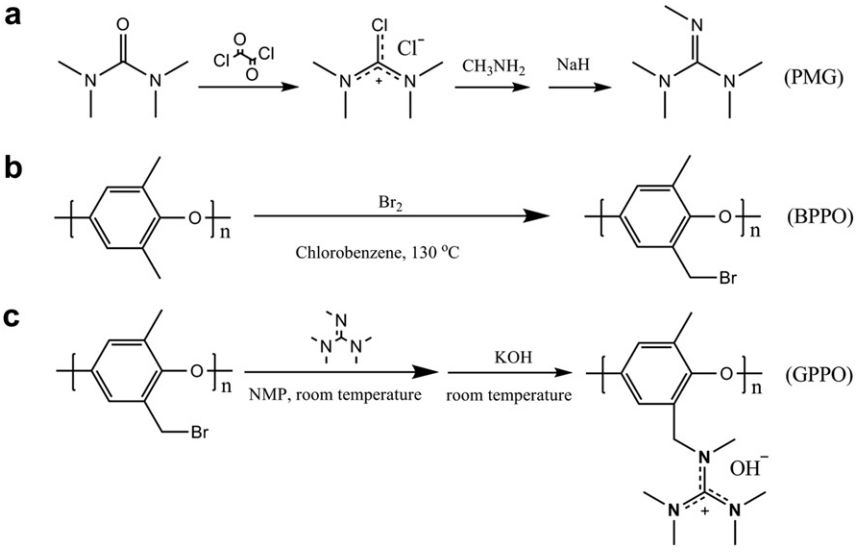


**Scheme 1.** The synthesis of the PMG quaternizing reagent and the BPPO and GPPO membranes.

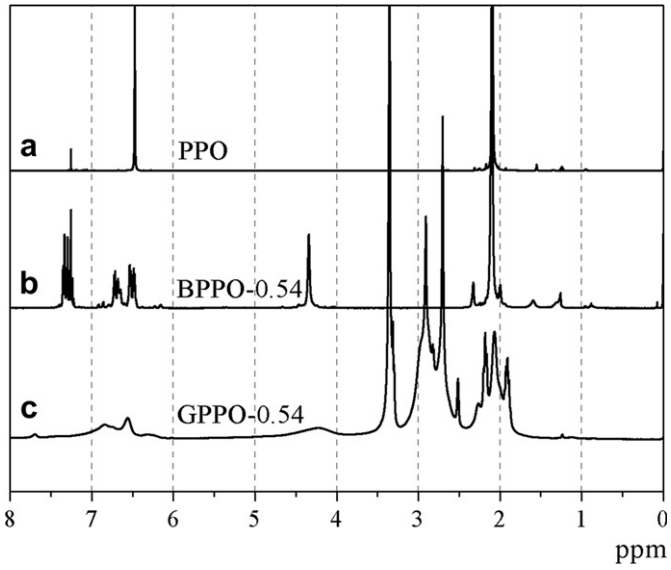


**Fig. 2.** The NMR spectra of (a) PPO, (b) BPPO-0.54 and (c) GPPO-0.54 membranes.

PPO, where the bands at 1610 $cm^{-1}$ and 1471 $cm^{-1}$ were assigned to the phenyl group vibrations [26]. New characteristic peaks at 743 $cm^{-1}$ were observed at Fig. 3b and c, for BPPO-0.30 and BPPO-0.54 respectively, which were attributed to the C—Br stretching vibration (confirmation of successful benzyl bromination) [27]. In the same way in Fig. 3d and e, for the GPPO analogues, new characteristic peaks at 1567 $cm^{-1}$ and 1677 $cm^{-1}$ were attributed to the C—N and C═N stretching vibration respectively [17,26] and confirmed the presence of guanidinium groups; the new broad peaks at 3415 $cm^{-1}$ were attributed to the —OH stretching vibration [28]. The degree of conversion was 100% as confirmed by the disappearance of the C—Br peak at 743 $cm^{-1}$.

During the preparation of BPPO, the addition of $Br_2$ was increased to raise the contents of $-CH_2Br$ groups (BPPO-0.05 to BPPO-0.54). Proof of this can be seen with the incremental increase in intensity of the C—Br band at 743 $cm^{-1}$ from Fig. 3b to Fig. 3c. In the same way, the increase in quaternary guanidinium group content from GPPO-0.05 to GPPO-0.54 was confirmed by the increased intensity of the 1567 and 1667 $cm^{-1}$ bands from Fig. 3d to Fig. 3e.

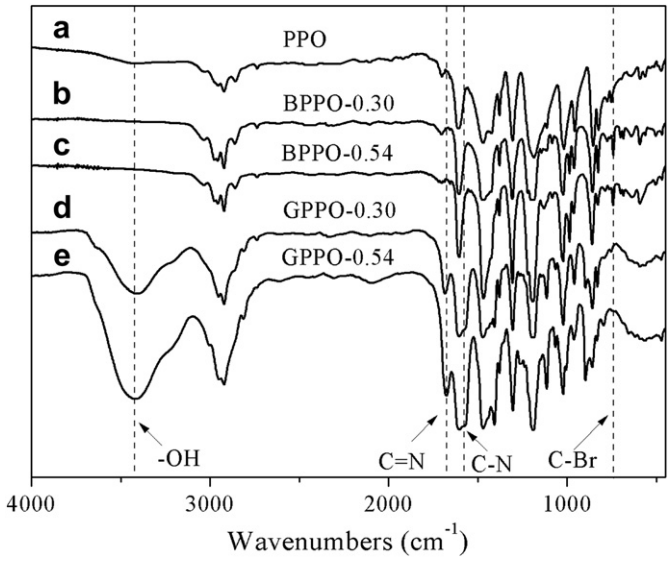


**Fig. 3.** The FT-IR spectra of (a) PPO, (b, c) BPPO-*X* and (d, e) GPPO-*X* membranes.

### 3.3. Ion exchange capacity (IEC), water uptake ($W_R$) and linear expansion ratio (LER)

The IEC, $W_R$ and LER of the GPPO-*X* membranes were measured under the same conditions and are summarized in Table 2. The IEC is one of the most important parameters in the characterization of ion-exchange membranes because it is an intrinsic measurement of the gravimmetric density of functional groups inside the membrane matrix. As shown in Table 2, the IEC values increased from 0.37 to 2.69 mmol $g^{-1}$ for GPPO-0.05 to GPPO-0.54. This is as anticipated as the IEC values of GPPO membranes should increase on increasing levels benzyl bromination as these groups, in the intermediate BPPO, are directly converted to guanidinium anion-exchange groups. The experimental IEC values closely matched the theoretical values and this is further confirmation of the complete reaction of the $-CH_2Br$ groups with PMG. In addition, the QPPO-0.42 QA benchmark membrane (theoretical IEC = 2.76 mmol $g^{-1}$) yielded an experimental IEC = 2.65 mmol $g^{-1}$ (approaches the value measured for GPPO-0.54).

As is well known, the water uptake is an important property for ion-exchange membrane because of the direct relationship between this parameter and the ion conductivity. For AAEMs specifically, the presence of water molecules is considered mandatory for facilitated hydroxide (or any anion) transport. However, too high a water uptake can result in the deterioration of the thermal, mechanical, and chemical stabilities of the membranes (and may also reduce the ionic conductivities by reducing the concentration of conductive species). $W_R$ and LER values for the GPPO-*X* AAEMs are presented in Table 2. As expected, $W_R$ and LER values increase with increasing IEC (GPPO-0.05 to GPPO-0.54) at a given temperature. The phenomenon is easily explained by the hydrophilicity of guanidinium groups. As again anticipated, when the temperature was increased to 80 °C, $W_R$ and LER values increased accordingly. Specifically, GPPO-0.54 has a water uptake of 98.7% and an LER of 45.0% LER at 80 °C, which was significantly higher than observed at 25 °C (77.1% and 25.0% respectively). It is clear that the membrane matrix will be affected by this severe swelling at the higher temperatures, leading to a positive feedback loop where the resulting increase in free space in membrane matrix, due to water adsorption, further aggravates swelling. For comparison, the $W_R$ (and LER) values of QPPO-0.42 increased from 100% to 430% (and from 38% to 75%) on increased temperature; these values are significantly higher than those exhibited by GPPO-0.54 (recall of comparable IEC). This is an important result and indicates that the guanidinium head-groups yield AAEMs that intrinsically swell less than the quaternary ammonium analogues. It was observed that GPPO-0.54 maintained considerable strength after immersion in water for 2 d at 80 °C,

**Table 2**
Ion exchange capacities, water uptakes and linear expansion ratios of the GPPO AAEMs.

| Sample | IEC (mmol $g^{-1}$) | | $W_R$ (%) | | LER (%) | |
|---|---|---|---|---|---|---|
| | Theoretical | Experimental | 25 °C | 80 °C | 25 °C | 80 °C |
| GPPO-0.05 | 0.39 | 0.37 | 6.1 | 14.8 | 2.5 | 2.5 |
| GPPO-0.09 | 0.74 | 0.69 | 10.9 | 17.1 | 3.8 | 3.8 |
| GPPO-0.22 | 1.45 | 1.20 | 13.1 | 30.2 | 6.3 | 7.5 |
| GPPO-0.30 | 1.83 | 1.71 | 32.0 | 51.5 | 10.0 | 12.5 |
| GPPO-0.42 | 2.32 | 2.23 | 49.9 | 72.9 | 12.5 | 18.9 |
| GPPO-0.54 | 2.72 | 2.69 | 77.1 | 98.7 | 25.0 | 45.0 |
| QPPO-0.42 | 2.76 | 2.65 | 100.6 | 430.1 | 37.5 | 75.6 |

while QPPO-0.42 was highly swollen and fragile under the same conditions.

### 3.4. Ionic conductivity

Herein, the ionic conductivities were examined by electrochemical impedance spectra (EIS – recorded in the frequency range of 10 Hz to 100 kHz and with a signal amplitude of 0.1 mA). Typical Nyquist plots for the GPPO AAEMs are presented in Fig. 4(a). The membrane resistances were obtained from the intercept on the Z′ axis in the low-frequency range. It can be seen that all Nyquist plots are similar and show a generic semicircle loop. The resultant ionic conductivities of the fully hydrated GPPO AAEMs are shown in Fig. 4(b). From GPPO-0.05 to GPPO-0.54, the conductivities of GPPO AAEMs increased from 11 to 71 mS $cm^{-1}$. This can again be anticipated considering the increased IEC (and water content). In comparison, QPPO-0.42 shows a hydroxide conductivity of only 44 mS $cm^{-1}$, which is much lower than observed for GPPO-0.54. Therefore, the higher alkalinity of the guanidinium groups has led to the desired improvement in ionic conductivity [17,29]; this is especially promising when considered alongside the reduction in AAEM swelling with this head-group chemistry. In addition, the

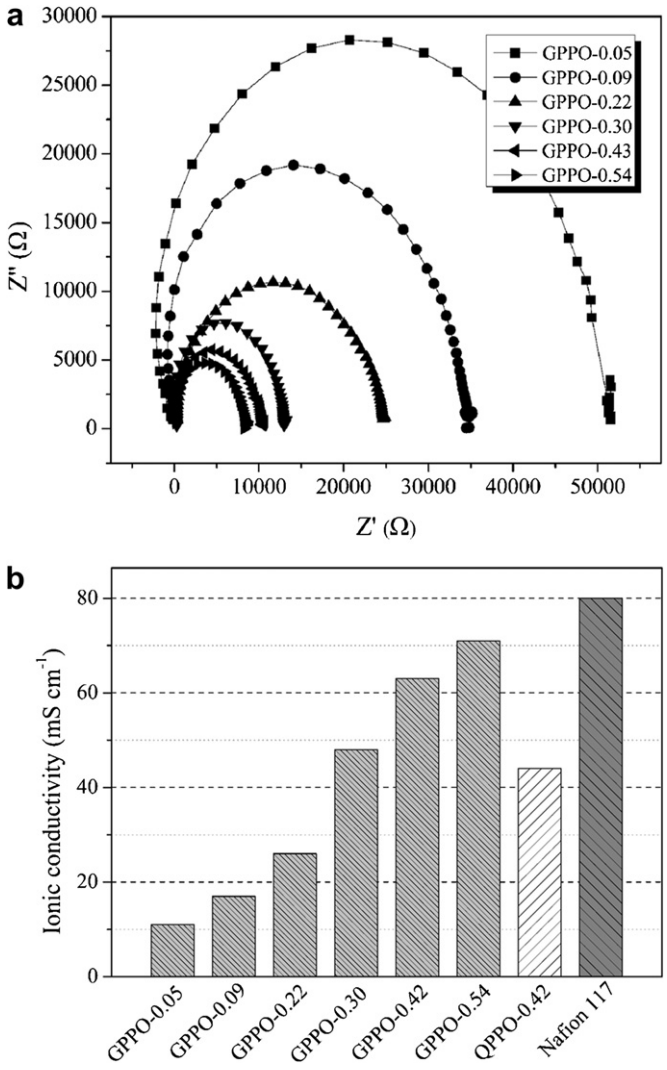


**Fig. 4.** (a) Representative Nyquist plots (Z″ versus Z′) from AC impedance spectroscopy measurements on the GPPO membranes. (b) The ionic conductivities of the GPPO AAEMs, QPPO-0.42 benchmark AAEM and Nafion117 benchmark PEM.

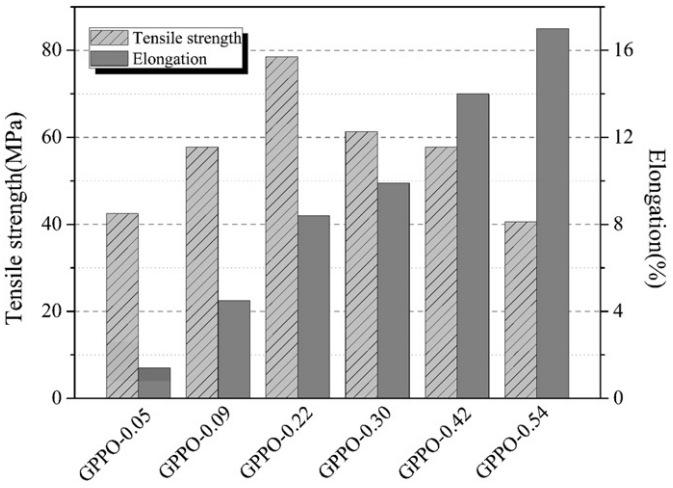


**Fig. 5.** The tensile strength (TS) and the elongation at the break ($E_b$) of the GPPO AAEMs.

$H^+$-conductivity of Nafion® 117 was measured at 80 mS $cm^{-1}$ when tested under the same conditions. This confirms recent reports by others [17,29] that the alkali anion conductivities of AAEMs can attain 60–90% of proton conductivities of PEMs such as Nafion® 117. The mobilities and diffusion constants of hydroxide anions are generally considered to be 33–50% of that of protons ($H^+$). From this viewpoint, the ionic conductivities of the GPPO membranes are extremely high and show great promise.

### 3.5. Mechanical properties

The mechanical properties of membranes are shown in Fig. 5. The tensile strength (TS) and elongation to break ($E_b$) values for the GPPO membranes were in the range of 52.5–78.5 MPa and 1.4%–17.0% respectively; these mechanical properties compare well to other reported ion-exchange membranes (even the Nafion® series of PEMs). For example, in our previous work, a series of organic–inorganic hybrid AAEMs based on PPO exhibited TS values of 20–27 MPa [30]. Meanwhile, Nicholas et al. prepared a series of highly cross-linked AAEMs which showed TS values of 10–30 MPa [31].

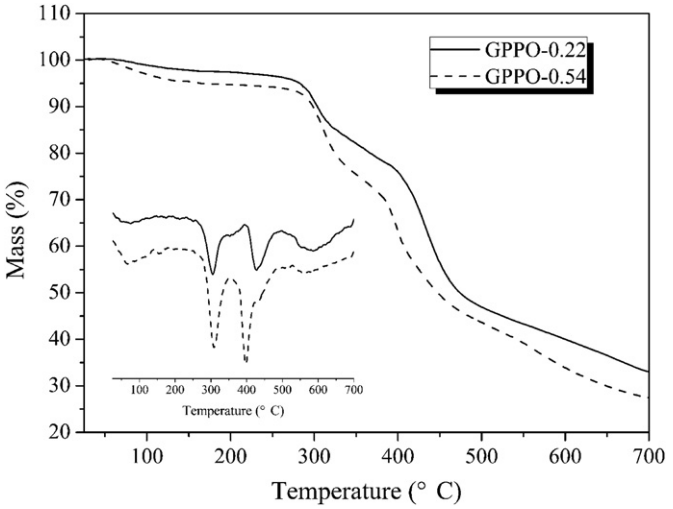


**Fig. 6.** The TGA and DTG of the GPPO AAEMs.

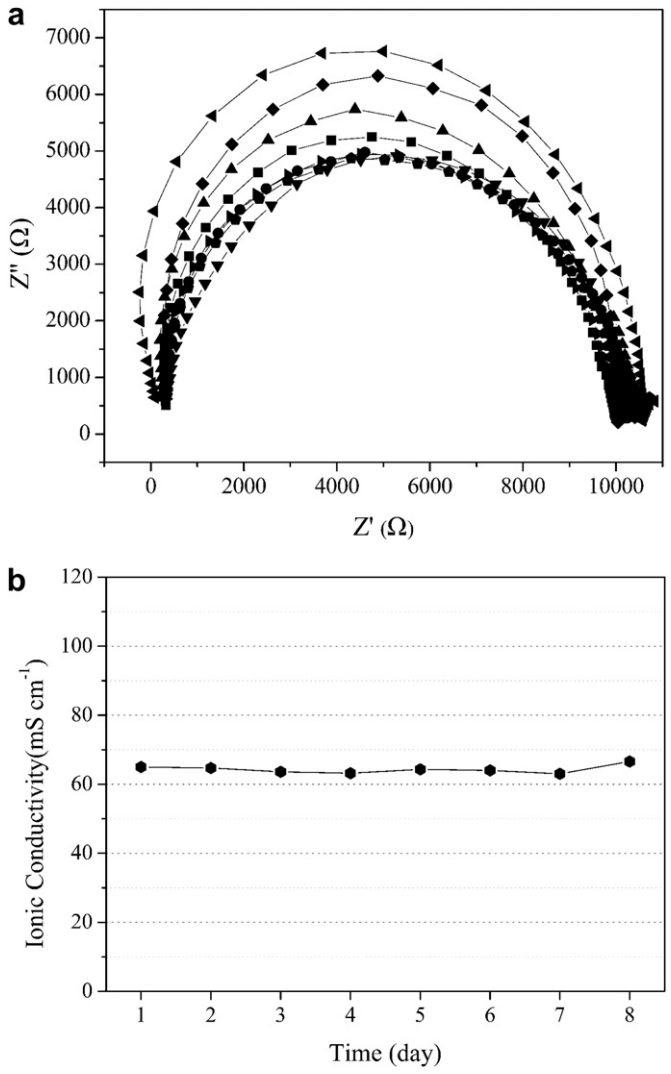


**Fig. 7.** (a) Representative Nyquist plots of $Z''$ versus $Z'$ from AC impedance spectroscopy measurements on GPPO-0.42 samples after immersion in aqueous KOH solution (1 mol $dm^{-3}$) at 25 °C. (b). The ionic conductivities of the GPPO AAEMs after immersion in aqueous KOH solution (1 mol $dm^{-3}$) at 25 °C for increasing lengths of time.

The mechanical properties of GPPO AAEMs directly depend on the IEC. As shown in Fig. 5, the TS values firstly increase and then decrease with the increasing contents of guanidinium groups, whilst the $E_b$ values show an ever-increasing trend. This result demonstrates that the presence of guanidinium groups of appropriate content enhances the mechanical properties of GPPO membranes. However, an excessive amount of quaternary guanidinium groups leads to too high water contents, which aggravates swelling and thereby decreases the mechanical properties of membranes (see $W_R$ and LER discussions above).

### 3.6. Thermal and alkaline stabilities

The thermo-gravimmetric analysis (TGA) and differential thermo-gravimmetric analysis (DTG) analyses of GPPO-0.22 and GPPO-0.54 AAEMs are shown in Fig. 6. Both GPPO AAEMs lost a small amount of mass from 50 °C to 120 °C, which was assumed to be due to the evaporation of absorbed water (and are therefore ignored in the following discussion). In addition, they both exhibited a start decomposition temperature of *ca.* 270 °C indicating the good short-term thermal stabilities of GPPO AAEMs. For comparison, the QA benchmark AAEMs exhibited a start decomposition temperature of *ca.* 200 °C [32]. DTG curves (inset to Fig. 6) were used to reveal more details about the thermal decomposition of GPPO AAEMs. The primary mass loss in the range of 270–350 °C was assigned to the decomposition of guanidinium groups [17]. Over 400 °C, the residues degraded further due to the decomposition of polymer main chains [32].

The GPPO AAEMs of reasonable IEC therefore showed excellent short-term thermal stabilities with high decomposition on-set temperatures ($T_d$ > 250 °C). As the typical working temperature of APEFCs is in the range 50–80 °C, the short-term thermal stabilities of the GPPO AAEMs appear promising. However, to get a measure of the more realistic (and fuel cell relevant) medium- to long-term alkaline stability of the GPPO AAEMs, GPPO-0.42 was chosen as an exemplar for further investigation. The GPPO-0.42 AAEM was immersed in aqueous KOH (1 mol $dm^{-3}$) solution for 8 d and the resulting Nyquist plots are presented in Fig. 7(a). All plots show a similar generic semicircle loop and some exhibit significant overlap. Moreover, the membrane resistances obtained (from the intercept on the $Z'$ axis in the low-frequency range) are also similar. The results suggest the GPPO AAEMs have good alkali stabilities. The resultant ionic conductivities were also recorded at increasing alkali immersion times (Fig. 7(b)). No obvious decrease in conductivity was observed even after 8 d of immersion. The results indicate that the GPPO AAEMs maintain their functional group chemistries under strongly alkaline conditions. Compared with GPPO AAEMs, the QA-AAEMs lost 20–40% of their functional groups under similar conditions [33,34]. The excellent alkali stability of GPPO AAEMs may derive from the presence of the π electron conjugated system of the pendant guanidinium groups (shown in Scheme 2), which allows the positive charge to be delocalized over one carbon and three nitrogen atoms; this clearly leads to the good thermal and alkali stabilities observed [17,29,35].

### 3.7. Fuel cell performance

GPPO-0.54 (thickness = 80 μm, IEC = 2.69 mmol $g^{-1}$) was used for initial beginning-of-life fuel cell performance testing (at 50 °C, supplied with fully humidified $H_2$ and $O_2$ gases at the anode and cathode respectively). The fuel cell performance data is shown in Fig. 8. As can be seen, the alkaline fuel cell exhibited an open circuit voltage (OCV) of 0.95 V, which was similar to a fuel cell using a QA-AAEM [36]. A peak power density of 16 mW $cm^{-2}$ at a current

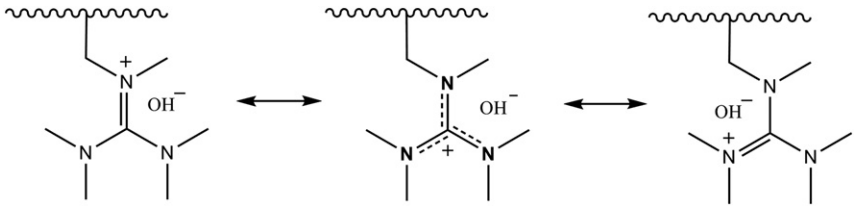


**Scheme 2.** The electron delocalization in the guanidinium functional head-groups.

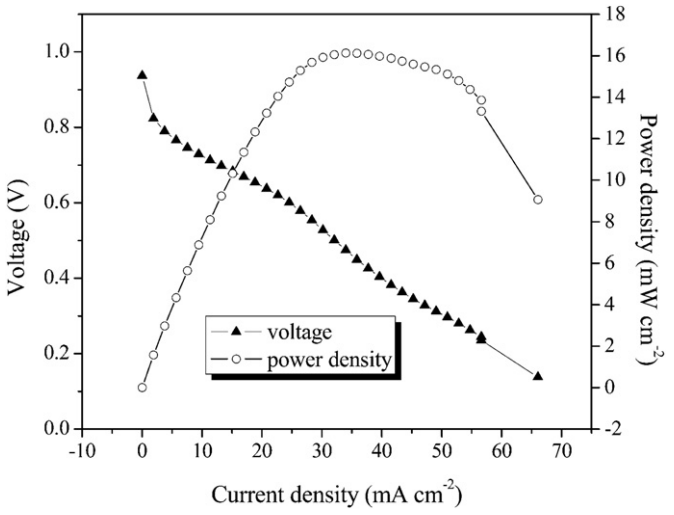


**Fig. 8.** Beginning-of-life polarization and power density curves of a $H_2/O_2$ fuel cell at 50 °C containing GPPO-0.54.

density of 34 mA cm$^{-2}$ was achieved. The value is comparable to that recorded for imidazolium-functionalized AAEM at 60 °C (16 mW cm$^{-2}$) [37] and higher than that of the QA PPO-based AAEM at 50 °C (9 mW cm$^{-2}$) [36]. However, the performance is surprisingly low when considering the high ex situ conductivities recorded (*cf.* the 180 mW cm$^{-2}$ that can be achieved with radiation-grafted QA AAEMs, of fully hydrated thicknesses of 80 μm and ionic conductivities of 30–60 mS cm$^{-1}$, tested with the same test conditions and on the same test equipment). The poor chemical compatibility between the quaternary ammonium alkaline ionomer used in the electrodes and the guanidinium-type membrane is a likely to be the cause of the poor performance observed. Chemical incompatibilities such as this can cause high contact resistances and poor MEA lamination (especially likely considering the difference in the $T_g$s of the ionomer and membrane). Also note that the prior performances using this ionomer are the end result from years of optimization work when used with the QA-AAEMs. This highlights the future requirement for the development of a guanidinium-type alkaline ionomer, if the full potential of this promising class of GPPO AAEMs is to be realized. This is now a research priority in our laboratories.

## 4. Conclusions

Alkaline Anion-Exchange Membranes (AAEMs) containing pedant guanidinium groups were prepared from poly(2,6-dimethyl-1,4-phenylene oxide) (PPO) via benzyl bromination followed by reaction with 1,1,2,3,3-pentamethylguanidine (PMG). The resulting AAEMs (GPPO) possessed remarkably high alkali anion conductivities (due to the high basicity of guanidinium groups) without excessive swelling. In addition, the GPPO AAEMs exhibit excellent short-term thermal and longer-term alkali stabilities due to the presence of the π electron conjugated system of the pendant guanidinium head-groups. The GPPO AAEMs exhibited high ion-exchange capacities (IECs) and excellent mechanical properties. Furthermore, the ex situ properties of the AAEMs can be optimized by varying the concentration of guanidinium groups. A high IEC exemplar AAEM was tested in a single cell $H_2/O_2$ fuel cell and yielded a beginning-of-life peak power density of 16 mW cm$^{-2}$. This work highlights the promise of guanidinium-type AAEMs for application in alkaline polymer electrolyte fuel cells (APEFC) and highlights that both membranes and ionomers (for electrode fabrication) need to be developed in parallel to fulfil this head-groups promise.

## Acknowledgements

This project was supported in part by the National Natural Science Foundation of China (Nos. 21025626, 20974106 and J1030412), the National Basic Research Programs (Nos. 2012CB932800, 2009CB623403). The University of Surrey researchers were supported by the UK's Engineering and Physical Sciences Research Council (grants EP/I004882/1 and EP/H025340/1).

## References

[1] J.R. Varcoe, R.C.T. Slade, Fuel Cells 5 (2005) 187–200.
[2] C.A. Schiller, F. Richter, E. Gulzow, N. Wagner, Physical Chemistry Chemical Physics 3 (2001) 2113–2116.
[3] R. Zeng, J. Handsel, S.D. Poynton, A.J. Roberts, R.C.T. Slade, H. Herman, D.C. Apperley, J.R. Varcoe, Energy & Environmental Science 4 (2011) 4925–4928.
[4] K. Matsuoka, Y. Iriyama, T. Abe, M. Matsuoka, Z. Ogumi, Journal of Power Sources 150 (2005) 27–31.
[5] E. Agel, J. Bouet, J.F. Fauvarque, Journal of Power Sources 101 (2001) 267–274.
[6] L. An, T.S. Zhao, S.Y. Shen, Q.X. Wu, R. Chen, International Journal of Hydrogen Energy 35 (2010) 4329–4335.
[7] M. Tanaka, M. Koike, K. Miyatake, M. Watanabe, Polymer Chemistry 2 (2011) 99–106.
[8] L.A. Adams, S.D. Poynton, C. Tamain, R.C.T. Slade, J.R. Varcoe, ChemSusChem 1 (2008) 79–81.
[9] J. Fang, P.K. Shen, Journal of Membrane Science 285 (2006) 317–322.
[10] G. Wang, Y. Weng, D. Chu, R. Chen, D. Xie, Journal of Membrane Science 332 (2009) 63–68.
[11] Y. Xiong, Q.L. Liu, Q.H. Zeng, Journal of Power Sources 193 (2009) 541–546.
[12] W.G. Figueroa, R. Raszkowski, W. Weiss, New England Journal of Medicine 288 (1973) 1096–1097.
[13] V. Neagu, I. Bunia, I. Plesca, Polymer Degradation and Stability 70 (2000) 463–468.
[14] A.A. Zagorodni, D.L. Kotova, V.F. Selemenev, Reactive and Functional Polymers 53 (2002) 157–171.
[15] S. Chempath, J.M. Boncella, L.R. Pratt, N. Henson, B.S. Pivovar, The Journal of Physical Chemistry C 114 (2010) 11977–11983.
[16] D.H.B. Ripin, pKa, in: Practical Synthetic Organic Chemistry, John Wiley & Sons, Inc., 2011, pp. 771–803.
[17] J. Wang, S. Li, S. Zhang, Macromolecules 43 (2010) 3890–3896.
[18] T. Xu, W. Yang, Journal of Membrane Science 190 (2001) 159–166.
[19] T. Xu, D. Wu, L. Wu, Progress in Polymer Science 33 (2008) 894–915.
[20] Z. Zhang, L. Wu, T. Xu, Journal of Membrane Science 373 (2011) 160–166.
[21] Y. Sone, P. Ekdunge, D. Simonsson, Journal of the Electrochemical Society 143 (1996) 1254–1259.
[22] J.R. Varcoe, R.C.T. Slade, Electrochemistry Communications 8 (2006) 839–843.
[23] J.R. Varcoe, R.C.T. Slade, E.L.H. Yee, S.D. Poynton, D.J. Driscoll, Journal of Power Sources 173 (2007) 194–199.
[24] R. Zeng, S.D. Poynton, J.P. Kizewski, R.C.T. Slade, J.R. Varcoe, Electrochemistry Communications 12 (2010) 823–825.
[25] V.J. Bauer, W. Fulmor, G.O. Morton, S.R. Safir, Journal of the American Chemical Society 90 (1968) 6846–6847.
[26] Y. Li, T. Xu, M. Gong, Journal of Membrane Science 279 (2006) 200–208.
[27] M.C. Dujardin, C. Cazé, I. Vroman, Reactive and Functional Polymers 43 (2000) 123–132.
[28] Y. Wu, C. Wu, T. Xu, F. Yu, Y. Fu, Journal of Membrane Science 321 (2008) 299–308.
[29] S. Gu, R. Cai, T. Luo, Z. Chen, M. Sun, Y. Liu, G. He, Y. Yan, Angewandte Chemie International Edition 48 (2009) 6499–6502.
[30] J. Luo, C. Wu, Y. Wu, T. Xu, Journal of Membrane Science 347 (2010) 240–249.
[31] N.J. Robertson, H.A. Kostalik, T.J. Clark, P.F. Mutolo, H.C.D. Abruña, a, G.W. Coates, Journal of the American Chemical Society 132 (2010) 3400–3404.
[32] L. Wu, T. Xu, D. Wu, X. Zheng, Journal of Membrane Science 310 (2008) 577–585.
[33] X. Lin, C. Wu, Y. Wu, T. Xu, Journal of Applied Polymer Science 123 (2012) 3644–3651.
[34] L. Wu, G. Zhou, X. Liu, Z. Zhang, C. Li, T. Xu, Journal of Membrane Science 371 (2011) 155–162.
[35] N.M.M. Mateus, L.C. Branco, N.M.T. Lourenco, C.A.M. Afonso, Green Chemistry 5 (2003) 347–352.
[36] A.L. Ong, S. Saad, R. Lan, R.J. Goodfellow, S. Tao, Journal of Power Sources 196 (2011) 8272–8279.
[37] F. Zhang, H. Zhang, C. Qu, Journal of Materials Chemistry 21 (2011) 12744–12752.